CrystEngComm

Accepted Manuscript

ROYAL SOCIETY OF CHEMISTRY

www.rsc.org/crystengcomm

CrystEngComm

RSCPublishing

ARTICLE

Towards the Epitaxial Growth of Silver on Germanium by Galvanic Displacement

Cite this: DOI: 10.1039/x0xx00000x

Received:,
Accepted :

DOI: 10.1039/x0xx00000x

www.rsc.org/

Sayed Youssef Sayed†‡

This work focuses on the synthesis and interfacial characterization of silver films grown on Ge(111) surfaces. The synthetic approach uses galvanic displacement, a type of electroless deposition that takes place in an efficient manner under aqueous and room temperature conditions. The case of silver-on-germanium has been widely studied and used for several applications, and yet a number of important fundamental questions remain in order to address the nature of these interfaces. Interfacial characterization reveals no evidence for the intermetallic nature of Ag-Ge interfaces and suggests the diffusion of silver into the germanium substrate. The texture nature of the grown silver films was investigated via pole figure x-ray diffraction (XRD) and cross-section nano-beam-diffraction transmission electron microscope (TEM) analyses, indicating the epitaxial growth of silver films on germanium lattices by galvanic displacement at ambient conditions.

1. INTRODUCTION

The integration of metals with semiconductor surfaces is currently employed in versatile applications, including integrated circuits,[1] optoelectronics,[2, 3] micro- and nano-electromechanical systems,[4, 5] sensing devices,[6] catalysis,[7] and others.[8, 9] Galvanic displacement (GD), a member of the electroless deposition family,[10-12] has gained much attention for interfacing metals with semiconductors.[13, 14] In this class of reactions, sufficiently oxidizing metal ions, with a redox potential more positive than that of substrate, are reduced spontaneously by electrons derived from the bonding electrons of the substrate lattice valence band. The reaction is accompanied by substrate dissolution and occurs in the absence of an external source of electric current or chemical reducing agents, as shown in Scheme 1. The result is metallic nanoparticles and films interfaced directly with the substrate surface.[15, 16] Galvanic displacement was found to be advantageous over the commonly used metal evaporation[17] and sputtering techniques[18] in terms of its simplicity, cost effectiveness, and production of films of controlled morphology and crystalline orientation.[2, 9, 11, 12, 19] For instance, ultra high vacuum and annealing conditions are required for evaporated gold to align epitaxially on silicon surfaces,[20] while, in the case of galvanic displacement, heteropeitaxial growth of metallic nanostructures on various silicon surfaces such as Si(111), Si(100), and Si nanowires occurs at ambient conditions.[12, 21]

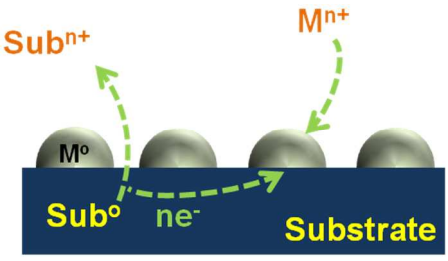

Scheme 1 Galvanic displacement process: the substrate act as the reducing agent and the source of electrons required for the reduction of metal ions on the semiconductor surface.

The growth of gold on silicon and germanium surfaces by galvanic displacement was studied comprehensively since the early reports of Balashova eta al.[22] and Krikshtopaitis et al.,[23] respectively. Through detailed X-rays photoelectron spectroscopy (XPS) and transmission electron microscopy (TEM) analyses,[12, 24, 25] both interfaces were characterized and identified as a mixture of intermetallic components sandwiched in between gold and the semiconductor surfaces. Galvanic displacement of silver on germanium has been studied intermittently for the synthesis of metal-semiconductor contacts[26] designed for versatile applications, including organic light emitting diodes (OLED),[27] and surface enhanced Raman spectroscopy (SERS),[16] for example. In an impact to the desired applications, most of the studies focused on

†Department of Chemistry, University of Alberta, Edmonton, AB, T6G 2G2, Canada. E-mail: sysayed@mit.edu
Electronic Supplementary Information (ESI) available: See DOI:10.1039/b000000x

controlling the shape and morphology of the synthesized structures. To date, however, the interfacial composition and the texture nature that would have a direct effect on the resulting electrical nature of these devices still remain unknown, whether there is perhaps heteroepitaxial film formation, or the presence of intermetallics, both of which are observed in the gold-on-germanium case.[24] In this paper, we focus upon the characterization of silver and germanium interfaces formed at room temperature by galvanic displacement through a variety of methods, including, X-ray photoelectron spectroscopy depth profiling, cross-sectional Auger electron spectroscopy (AES), cross-sectional transmission electron microscopy, and detailed X-ray diffraction (XRD) measurements to identify and fully understand the nature of these interfaces.

2. Experimental Section

Generalities: Unless otherwise noted, all experiments were performed under ambient laboratory conditions. Ge(111) (p-type, Ga-doped, ρ = 0.24-0.33 Ω·cm, 500 μm thickness) wafers were purchased from MTI Corporation. $AgNO_3$ were purchased from Strem Chemicals.

Pretreatment of Germanium Substrates: All wafers were diced into 0.8 cm^2 pieces with a diamond scriber. Germanium shards were degreased in a methanol ultrasonic bath for 15 min, in boiling dichloromethane for 10 min, and then a methanol ultrasound bath for 10 min. The oxide layer was removed with a solution of 3.5M NH_4OH (aq) for 5 min,[28] followed by rinsing samples with DI water and dried with a stream of nitrogen.

Metal Deposition: Germanium shards were immersed in either the desired aqueous silver salt solutions or the metallic salt and 5% hydrofluoric acid (aq) in a Teflon beaker. After metal deposition, the sample was thoroughly rinsed with water and dried under a nitrogen stream.

Surface Characterization**:** The silver nanostructures on the germanium surfaces were characterized by scanning electron microscopy (SEM). SEM (Hitachi S-4800 FE-SEM) images of metallic nanostructures were typically performed with an electron energy of 20 keV. Auger measurements were carried out using a JAMP-9500F Auger microscope (JEOL). The accelerating voltage and the emission current for both the SEM and Auger imaging were 15 KV and 8 nA, respectively.

The crystalline nature of the metallic upper layer was analyzed by X-ray diffraction (XRD). The out-of-plane orientation, the theta (θ)-2theta (2θ) scan, was investigated using a Bruker D8 Discover diffractometer equipped with a 1/4 Eulerian cradle, Cu X-ray tube, a 1 mm collimator, and a 2D Hi-Star proportional detector. The detector was placed 15 cm from the sample. The texture of the films and the in-plane orientation were investigated using XRD pole figure analyses. To capture the whole (111) pole figure intensity distribution, the sample was tilted at different psi "ψ" angles: 90^o, 60^o, 19.5^o; chi "χ" = $90^o - \psi$. At each tilting angle the sample was rotated azimuthally from phi (φ) = 0^o to 360° with a 5^o scan step (72 frames for each ψ).

XPS (Kratos Analytical, Axis- Ultra) was performed using monochromatic Al Kα (1486.6 eV) source. The pressure in the XPS chamber was ~8 x 10^{-10} Torr at time of measurement. For sputtering, 5 keV Ar^+ ions were used with a beam current of 0.9 μA on the sample. The instrument was calibrated on the basis of the C 1s peak. The Ag 3d positions were also calibrated using sputtered Ag film.

High resolution TEM (HRTEM) images and nanobeam diffraction (NBD) patterns (with a probe of ~5 nm) were recorded on a Shottky-emission 200 kV JEOL 2200FS TEM/STEM microscope with in-column energy filter equipped with a high tilt cryo-polepiece, and a cold-field-emission 300 kV Hitachi HF3300 TEM/STEM microscope with a post-column energy filter.

Cross-sectional TEM samples of Ag/Ge(111) were prepared on a Hitachi NB5000 Focused Ion & Electron Beam System. A 40 keV Ga ion beam was used to produce a thin section about 200 nm thick, and Ar ion milling was then used for final thinning and cleaning of the surface. Ion milling was done at low temperature (with LN_2 cooling) at a 6° milling angle, and with a two-step process: voltage/current of 1 kV/3 mA for thinning and 0.5 kV/3 mA for final polishing.

3. RESULTS AND DISCUSSION

Galvanic displacement occurs spontaneously when a semiconductor substrate is immersed in a solution of sufficiently oxidizing metal ions. When an oxide-free shard of Ge(111) is immersed in an aqueous solution of 0.5 mM $AgNO_3$ + 5% HF for 15 min, a silver film of ca. 40 – 50 nm in thickness (Figure 1a-b) is formed according to equations (1) and (2):[24]

Anodic: $Ge \rightarrow Ge^{4+} + 4\ e^-$ $\quad E^o_{Ge^{4+}/Ge} = 0.12$ V vs. NHE (1)

Cathodic: $Ag^+ + e^- \rightarrow Ag^o(s)$ $\quad E^o_{Ag^+/Ag} = 0.79$ V vs. NHE (2)

Longer immersion times result in the growth of complex silver nanostructures.[19] The presence of an acid (HF) is essential to dissolve the insulating oxide that forms during the displacement process and would prevent direct contact of metal atoms on germanium surfaces.[11] The importance of a well-defined and oxide-free metal-semiconductor interfaces correlates to the necessity of low defect densities, high interfacial adhesion, and good electrical connectivity.[15, 29]

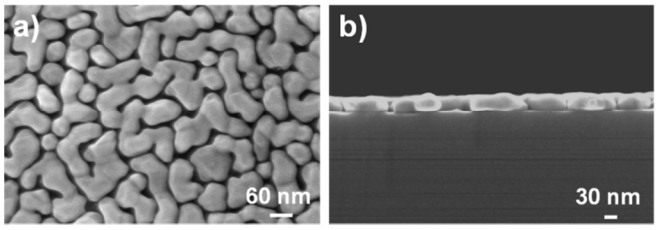

Fig. 1 Plan view (a) and cross-sectional (b) SEM images for silver nanostructures formed after 15 min immersion of a Ge(111) shard in 0.5 mM $AgNO_3$ (aq) + 5% of HF (aq).

Exploring the Ag-Ge interface is imperative to characterize and understand its interfacial bonding. Therefore, we performed XPS depth profiling as shown in Figure 2. The predictable photoemission peaks, arising from Ag $3d_{5/2}$ (368.4 eV), Ge 3d (29.5 eV) O 1s (531.2 eV), and C 1s (284.8 eV), are observed, (Supporting Information). XPS depth profiling involves measuring the binding energy (BE) of the newly exposed surface after Ar sputtering. As a result, it indicates and monitors changes in surface atomic identity across the examined layer. As shown in Figure 2, at 0 min of sputtering, the Ag $3d_{5/2}$ peak at 368.4 eV is visible, and corresponds to metallic Ag.[30] After 14 min, all the silver is removed. Following a transitional length of time of 4.5 min sputtering, the initial peak appears to shift only a very small amount, ~0.1 eV to a higher binding energy, to 368.5 eV. Small shifts in XPS could be due to a variety of factors, including final state effects in nanostructured metals, and others.[31] Hence, it is hard to conclude that this small shift in binding energy is meaningful in pointing

towards the existence of interfacial intermetallics involving silver. Yet, the cross-sectional interface between silver and germanium didn't show other new components in the nano-beam (20 nm) selected area electron diffraction (SAED) pattern (*vide infra*).

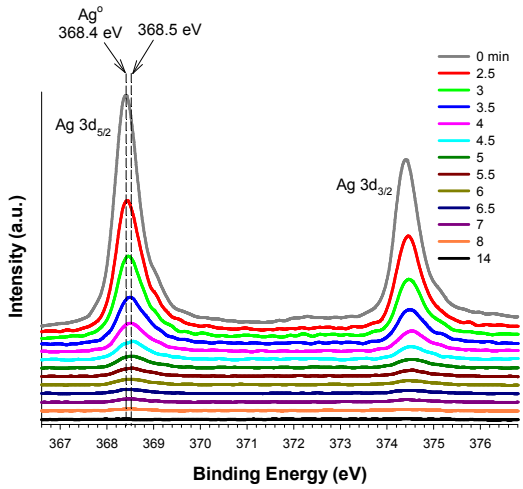

Fig. 2 Ag 3d XPS spectra of Ag on Ge(111), formed by immersion in 0.5 mM $AgNO_3$ + 5 % HF (aq), at different Ar^+ sputtering time intervals.

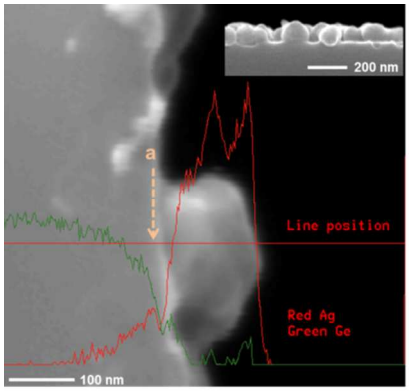

Fig. 3 Scanning Auger electron line-profile spectra of Ag on Ge(111) superimposed on the cross-sectional SEM images taken during the line-profile scanning processes. Ge and Ag line profiles are represented in green and red colors, respectively. The inset is a cross-section SEM image of Ag on Ge(111).

In correlation to the metal-semiconductor interfacial interactions, we need to investigate whether elemental diffusion occurs at the interface or not. Addressing this point will allow further understanding of the Ag-Ge system. In the case of evaporated Ag on Ge, Mehrer and co-workers[32] have studied the diffusion of Ag into the germanium substrate at higher temperatures (> 900 °C), and have shown a diffusivity of 0.02 nm^2 s^{-1} at 973 K via a dissociative-diffusion mechanism. The growth of noble metals on semiconductor surfaces by galvanic displacement exhibits room temperature behaviors such as epitaxial growth, and interfacial intermetallic formation[12] observed, however, at very high annealing temperature in the case of sputtered or evaporated films.[20, 32] Cross sectional Auger electron line profile analysis can provide a vision for the interfacial diffusion (Figure 3). Following the Ge Auger line profile, it is clear that the Auger intensity starts to decrease at position "a", indicating the interface between the silver and germanium substrate. The decay of the Ge intensity from point "a" to the top of the silver layer indicates either Ge diffusion into the silver layer or the existence of insistently surface oxides, in spite of the copious rinsing. Interestingly, the silver Auger line profile did not show an abrupt decrease at the interface (position a), however, it decays over a span of ~ 100 nm, indicating a possible diffusion of the Ag atoms into germanium, perhaps via a dissociative diffusion mechanism.

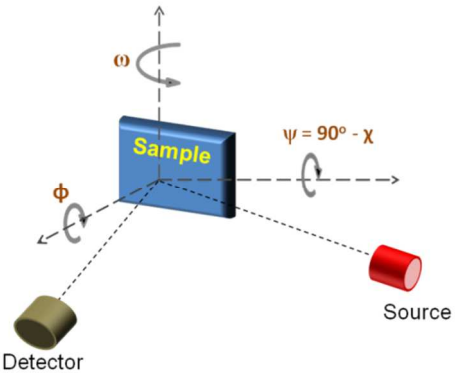

Scheme 2 Schematic diagram showing the experimental set up used in the in- and out-of-plane orientation analyses by X-ray diffraction. The pole figure was constructed by rotating the sample 360° along the azimuthal axis "φ" at different chi "χ" angles (ψ = 90° – χ). The sample was aligned vertically as shown in the figure at ψ = 90° (χ = 0°).

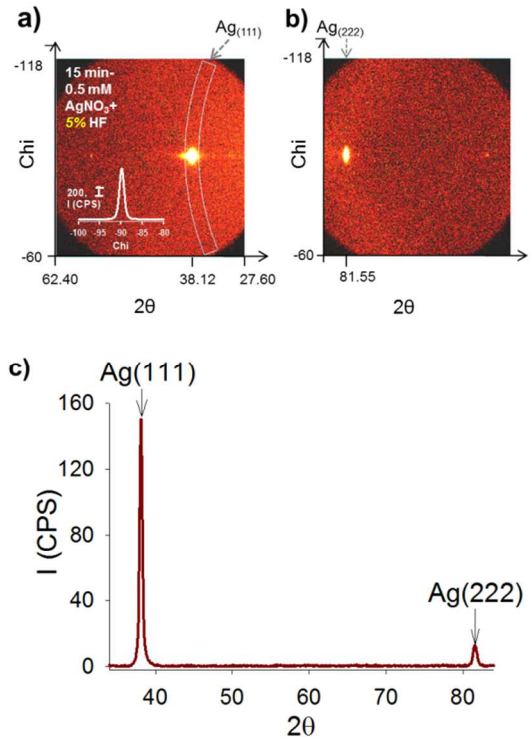

Fig. 4 XRD data observed from silver nanostructures on Ge(111) prepared after a 15 min immersion of a germanium shard in 0.5 mM $AgNO_3$ (aq) + 5% HF (aq). (a, b) 2D XRD frames observed in the 2θ range of 27.6-48.2°, and 60.9 – 85.83°, respectively. (c) θ-2θ scan.

To understand the nature of the grown silver films and their characteristics (crystalline orientation, preferred orientation,

epitaxy, etc.), we carried out detailed 2D X-ray diffraction analyses, allowing the acquisition of 2θ Bragg diffractions over a wide range of chi (χ) angles simultaneously (Scheme 2).[33] Hence, diffractions from a large fraction of planes aligned with different chi angles to the substrate surface can be acquired, important for samples with a preferred orientation and texture.[33] In Figure 4, panels a and b represent 2D X-ray diffraction frames acquired while probing the out-of-plane orientations of a silver film prepared after a 15 min immersion of an oxide-free germanium shard in 0.5 mM $AgNO_3$ (aq) + 5% HF (aq). Within a 2D frame, diffractions from families of planes diffracting in the investigated range of 2θ are acquired. As can be seen in Figures 4a and 4b, there are only two diffraction spots observed at 2θ = 38.12° and 81.55°, corresponding to diffractions from Ag(111) and Ag(222) planes, respectively.[34] Localized high intensity diffraction patterns of spots, resulting from planes of similar chi values, are diffractions that result from a film of a preferred orientation.[35] Polycrystalline films characterized by their random crystalline orientation would result in uniformly distributed intensities along Debye diffraction rings.[35]

The degree of alignment of the silver grains with the underlying germanium lattices can be revealed from the integration of the diffraction intensity at 2θ = 38.12° as a function of chi. The intensity-chi plot inserted in Figure 4a represents diffractions along the chi scale, an advantage of 2D XRD. The FWHM of the observed peak is 1.48. A small FWHM within the intensity-χ plot reveals a greater degree of ordering of the Ag(111) planes with respect to the Ge(111) surface plane (Supporting Information, Figures S2 and S3). Larger FWHM values and spread of diffractions on the chi scale indicate the existence of (111) planes that are not parallel to the substrate surface.[35] XRD θ-2θ scans are essential in defining the out-of-plane orientation of the grown metallic layer; the preferred *hkl* growth direction, which is parallel to the substrate surface normal and is of the same *hkl* identity of the planes preferably parallel to the substrate surface. XRD θ-2θ scan, probing the out-of-plane orientation of silver films (Figure 4c), is constructed by integrating the intensity of diffraction patterns observed from diffraction frames covering a 2θ scale in the range of 2.5-112°, acquiring diffractions from all silver planes. Only diffractions from Ag(111) and Ag(222) planes are acquired, indicating that the only planes parallel to the substrate surface are the (111) planes – the formation of highly textured silver film on the Ge(111) surface. Hence, the XRD θ-2θ scan indicates the <111> direction as the out-of-plane growth direction, and the Ag(111)//Ge(111) as the out-of-plane relationship.

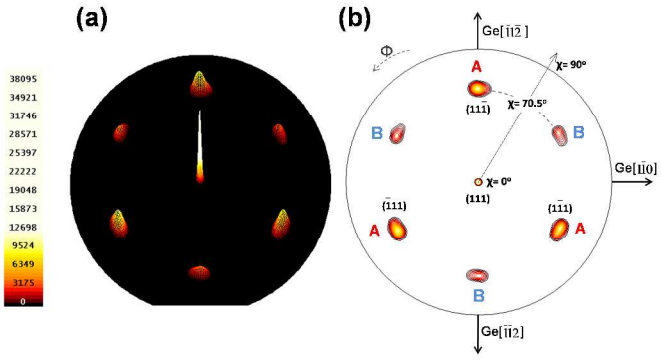

Fig. 5 (111) X-ray pole figures for Ag film, on Ge(111) substrate, produced after a 15 min immersion of a germanium substrate in 0.5 mM $AgNO_3$ (aq) solution containing 5% HF (aq). The (111) surface and contour pole figures are represented in (a) and (b), respectively. The pole figures were obtained by setting 2θ equals to the angle of diffraction from the Ag(111) planes (2θ = 38.12°) and collecting the diffraction intensity while rotating the sample azimuthally at different tilting angles (χ).

Although of the preferential growth along the <111> directions, the crystalline orientation may exhibit a random in-plane orientation (azimuthal direction).[36] Highly textured materials can be of either fiber or epitaxial texture, both of which can give seemingly similar θ-2θ scans. Films, whose crystallites are characterized by their random in-plane orientation around the texture axis, are of fiber texture.[36, 37] On the other hand, regular in-plane orientation is characteristic of epitaxially grown films. Identifying the texture nature of the grown films requires investigating the in-plane orientation of the crystallites. In-plane information can be provided from pole figures constructed by accumulating the diffraction intensities while rotating a sample azimuthally (360° along the rotation angle (φ)) at different chi angles (χ) and constant 2θ, corresponding to the plane of interest.[37] The three types of texture (random, fiber, and epitaxial) can be differentiated by their distinguishing pole figure. Polycrystalline films result in featureless pole figures, while fiber and epitaxial films are characterized by their ring diffraction pattern surrounding the pole figure central point, and defined diffraction spots at certain (Φ, χ) positions on the pole figure, respectively.[38]

The (111) surface and contour pole figures for the silver film grown on Ge(111) from (0.5 mM $AgNO_3$ (aq) + 5% HF (aq)) solution are shown in Figures 5a, and 5b, respectively. The diffraction peak at χ = 0° results from Ag(111) planes aligned parallel to the substrate surface. In a cubic system, the angle between the (111) plane and each of the ($\bar{1}$11), (1$\bar{1}$1), and (11$\bar{1}$) planes is 70.5°. In Figure 5, discrete diffraction spots are observed at χ = 70.5°, consequently, indicating the epitaxial alignment of the silver film. However, for face centered cubic (fcc) systems, three equally spaced diffraction spots are expected to be observed. The existence of six diffraction spots at χ = 70.5° (Figure 5) reveals the existence of two types of epitaxy or in-plane epitaxial textures denoted as "A" and "B" with B orientation of an intensity equals to ~ ¼ of that of A and is rotated 180° relative to the A orientation. The two epitaxial relationships for A and B orientations are Ag(111)[$\bar{1}$1 2]//Ge(111)[$\bar{1}$1 2], and Ag(111)[$\bar{1}$ 1 2]//Ge(111)[$\bar{1}$ 1 2], respectively. The existence of two epitaxial in-plane orientations has been observed for Au on silicon surfaces,[39] and was related to two possible alignments of gold atoms with the underlying silicon substrate – the epilayer is overlaying either six or three silicon atoms (in the second topmost substrate layer), resulting in a higher diffraction intensity possibly for the in-plane orientation with six underlying silicon atoms (Figure S10 in the Supporting Information).

In order to further prove the heteroepitaxial nature of the silver films, we used the precision of the transmission electron microscope (TEM). Figure 6a shows a cross-sectional high resolution TEM image for a silver-germanium interface prepared via the immersion of a germanium shard in a mixture of 0.5 mM $AgNO_3$ (aq) + 5% HF (aq) for 15 min. Figure 6b and 6c are nanobeam diffraction patterns observed from top silver and bulk germanium regions, respectively. The fact that both patterns have the same [11 $\bar{2}$] zone axis indicate the parallel nature of the *112* family of planes, {112}, for both Ag and Ge. Interestingly, the diffraction pattern taken from the Ag-Ge interface, region "2" in panel 6a, shows some common alignments for both Ag and Ge (Figure 6d). Firstly, the common [11 $\bar{2}$] zone axis indicates the alignment of the {112} planes of both the germanium substrate and the germanium-silver interface, which in turns results in identical alignment for the top grown silver layer

(panel 6b). Secondly, for each germanium Bragg diffraction spot there is a silver Bragg diffraction spot of identical orientation. The germanium diffraction spots arising from the $(\bar{1}\,1\,\bar{1})$, (220) and $(13\bar{1})$ planes are due to the substrate single crystal nature. Evidently, silver shows diffraction spots from the same planes, indicating the single crystal nature of the silver epilayer and the parallel alignment for the silver $(\bar{1}\,1\,\bar{1})$, $(13\bar{1})$ and (220) planes with the germanium $(\bar{1}\,1\,\bar{1})$, $(13\bar{1})$ and (220) planes, respectively. Hereafter, the interfacial analyses provided by the nanobeam diffraction patterns from silver film on germanium substrate indicate the epitaxial growth of silver on germanium and the Ag(111) [$11\,\bar{2}$]//Ge(111) [$11\,\bar{2}$] epitaxial relationship, which is in agreement with the XRD analyses.

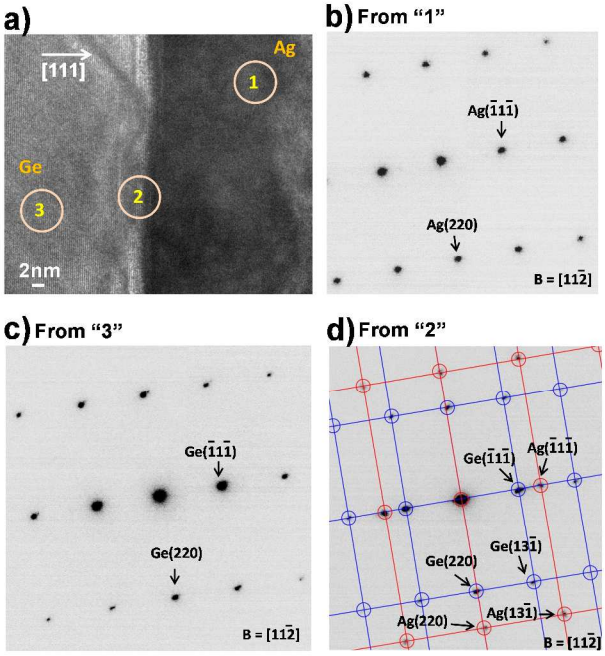

Fig. 6 Cross-sectional high resolution transmission electron micrograph for silver-on-Ge(111), formed by immersing the germanium substrate in 0.5 mM $AgNO_3$ (aq) + 5% HF (aq) for 15 min. (b-d) Nanobeam diffraction patterns (probe ≈ 5 nm) taken along the [$\bar{1}$ 12] zone axis from three different areas: (b) from top silver area marked by 1 in image "a", (c) from germanium substrate (area marked 3 in image "a"), and (d) from the silver-germanium interfacial area marked by 2 in image "a". Red and blue lines correspond to silver and germanium planes, respectively.

4. CONCLUSIONS

Silver nanostructures were interfaced on germanium surfaces via galvanic displacement mechanism from aqueous silver nitrate solutions containing hydrofluoric acid as an oxide etching agent. The existence of interfacial intermetallics was not observed either by XPS depth profile or cross-section TEM analyses. Scanning Auger electron microscopy did not show an abrupt vanish of the silver intensity at the interface, revealing possible silver diffusion into germanium. The grown silver films were investigated by using detailed XRD analyses. The out-of-plane θ-2θ scans have shown evidence for highly textured films, which may be grown epitaxially on Ge(111). Pole figure analyses investigated the in-plane orientation of silver crystallites and showed evidence for their heteroepitaxial nature. The epitaxial behavior was further proved by cross-sectional TEM investigations, involving nanobeam diffraction analyses. The epitaxial relationship observed from the pole figure analyses agrees with what was observed from the nanobeam diffraction pattern; Ag(111) [$11\,\bar{2}$]//Ge(111) [$11\,\bar{2}$].

Acknowledgements

This work was supported by the Alberta Innovates. I am also thankful for the technical support at the Alberta Centre for Surface Engineering and Science (ACSES). I thank professor Jillian Buriak for the fruitful discussion and support.

Notes and references

‡Permanent Address: Chemistry Department, Faculty of Science, Cairo University, Cairo, Egypt.

1. M. Leong, B. Doris, J. Kedzierski, K. Rim and M. Yang, *Science*, 2004, 306, 2057-2060.
2. R. Chen, D. Li, H. Hu, Y. Zhao, Y. Wang, N. Wong, S. Wang, Y. Zhang, J. Hu, Z. Shen and Q. Xiong, *Journal of Physical Chemistry C*, 2012, 116, 4416-4422.
3. T. Ootsuka, Z. X. Liu, M. Osamura, Y. Fukuzawa, N. Otogawa, Y. Nakayama, H. Tanoue and Y. Makita, *Materials Science and Engineering B-Solid State Materials for Advanced Technology*, 2005, 124, 449-452.
4. X. D. Li, B. Bhushan, K. Takashima, C. W. Baek and Y. K. Kim, *Ultramicroscopy*, 2003, 97, 481-494.
5. L. Magagnin, R. Maboudian and C. Carraro, *Electrochemical and Solid State Letters*, 2001, 4, C5-C7.
6. K. Q. Peng, X. Wang and S. T. Lee, *Applied Physics Letters*, 2009, 95.
7. J. Kye, M. Shin, B. Lim, J. W. Jang, I. Oh and S. Hwang, *ACS Nano*, 2013, 7, 6017-6023.
8. T. Mokari, E. Rothenberg, I. Popov, R. Costi and U. Banin, *Science*, 2004, 304, 1787-1790.
9. A. Lahiri, R. Wen, S. Kuimalee, A. Chowdhury, S. I. Kobayashi, L. Zhang, P. Wang and Y. Fang, *Journal of Physics D: Applied Physics*, 2013, 46.
10. G. Oskam, J. G. Long, A. Natarajan and P. C. Searson, *Journal of Physics D-Applied Physics*, 1998, 31, 1927-1949.
11. S. Y. Sayed and J. M. Buriak, *ACS Applied Materials & Interfaces*, 2010, 2 (12), 3515–3524.
12. S. Y. Sayed, F. Wang, M. Mallac, A. Meldrum, R. F. Egerton and J. M. Buriak, *ACS Nano*, 2009, 3, 2809-2817.
13. Y. G. Sun and G. P. Wiederrecht, *Small*, 2007, 3, 1964-1975.
14. J. G. Zhang, Y. Gao, T. Hanrath, B. A. Korgel and J. M. Buriak, *Chemical Communications*, 2007, 1438-1440.
15. C. Carraro, R. Maboudian and L. Magagnin, *Surface Science Reports*, 2007, 62, 499-525.
16. P. R. Brejna, P. R. Griffiths and J. Yang, *Appl Spectrosc*, 2009, 63, 396-400.
17. E. Piscopiello, L. Tapfer, M. V. Antisari, P. Paiano, P. Prete and N. Lovergine, *Physical Review B*, 2008, 78, 0353051 - 0353057.
18. H. Arakaki, K. Ohashi and T. Sudou, *Semiconductor Science and Technology*, 2004, 19, 127-132.

19. M. Aizawa, A. M. Cooper, M. Malac and J. M. Buriak, *Nano Letters*, 2005, 5, 815-819.
20. Y. Yokota, H. Hashimoto, N. Saito and H. Endoh, *Japanese Journal of Applied Physics Part 2-Letters*, 1986, 25, L168-L170.
21. S. Warren, A. Reitzle, A. Kazimirov, J. C. Ziegler, O. Bunk, L. X. Cao, F. U. Renner, D. M. Kolb, M. J. Bedzyk and J. Zegenhagen, *Surface Science*, 2002, 496, 287-298.
22. N. A. Balashova, V. V. Eletskii and V. V. Medyntsev, *Elektrokhimiya*, 1965, 1, 274-278.
23. I. B. Krikshtopaitis and Z. P. Kudzhmauskaite, *Elektrokhimiya*, 1971, 7, 1579-1581.
24. L. Magagnin, R. Maboudian and C. Carraro, *Journal of Physical Chemistry B*, 2002, 106, 401-407.
25. L. Y. Zhao, A. C. L. Siu, J. A. Petrus, Z. H. He and K. T. Leung, *Journal of the American Chemical Society*, 2007, 129, 5730-5734.
26. S. Barth, J. J. Boland and J. D. Holmes, *Nano Lett*, 2011, 11, 1550-1555.
27. C. Cioarec, P. Melpignano, N. Gherardi, R. Clergereaux and C. Villeneuve, *Langmuir*, 2011, 27, 3611-3617.
28. H. Okumura, T. Akane and S. Matsumoto, *Applied Surface Science*, 1998, 125, 125-128.
29. L. A. Porter, H. C. Choi, A. E. Ribbe and J. M. Buriak, *Nano Letters*, 2002, 2, 1067-1071.
30. M. Romand, M. Roubin and J.-P. Deloume, *Journal of Solid State Chemistry*, 1978, 25, 59-64.
31. M. Aizawa and J. M. Buriak, *Journal of the American Chemical Society*, 2006, 128, 5877-5886.
32. H. Bracht, N. A. Stolwijk and H. Mehrer, *Physical Review B*, 1991, 43, 14465-14477.
33. *Bruker Axs Inc., Bruker Advanced X-Ray Solutions: General Area Detector Diffraction Systems (GAADS)*, GAADS User's Manual, Madison.
34. *Joint Committe for Powder Diffraction Standards (JCPDS), File Number: 1-1174.*.
35. S. L. Liew, B. Balakrisnan, C. S. Ho, O. Thomas and D. Z. Chi, *Journal of the Electrochemical Society*, 2007, 154, H9-H12.
36. F. Tang, T. Parker, G. C. Wang and T. M. Lu, *Journal of Physics D-Applied Physics*, 2007, 40, R427-R439.
37. M. Birkholz, *Thin Film Analysis by X-Ray Scattering*, WILEY-VCH Verlag Gmbh & Co. KGaA, Weinheim, 2006.
38. C. Detavernier, A. S. Ozcan, J. Jordan-Sweet, E. A. Stach, J. Tersoff, F. M. Ross and C. Lavoie, *Nature*, 2003, 426, 641-645.
39. P. Prodhomme, S. Warren, R. Cortès, H. F. Jurca, F. Maroun and P. Allongue, *ChemPhysChem*, 2010, 11, 2992-3001.

TOC:

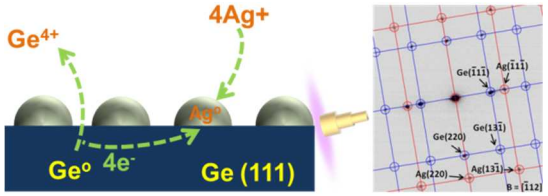

Interfacial Investigation for the epitaxial growth of Ag on Ge by galvanic displacement.